Heliyon 8 (2022) e11974

Contents lists available at ScienceDirect

Heliyon

journal homepage: www.cell.com/heliyon

Research article

Graphene-maleic anhydride-grafted-carboxylated acrylonitrile butadiene-rubber nanocomposites

Bismark Mensah *, Johnson Kwame Efavi, David Sasu Konadu, Gloria Pokuaa Manu

Department of Materials Science and Engineering, CBAS, University of Ghana, Legon, Ghana

ARTICLE INFO

Keywords:
Graphene sheets
Reduced graphene oxide
Maleic anhydride
Ethylene propylene rubber
Carboxylated acrylonitrile butadiene rubber
Mechanical strength and thermal degradation resistance

ABSTRACT

Ethylene-propylene grafted-maleic anhydride (EPR-g-MA) and a pure maleic anhydride (MA) were separately used to compound carboxylated acrylonitrile butadiene-rubber (XNBR) together with reduced graphene oxide (G) to form nanocomposites, by using melt compounding technique. The G-sheets in the presence of MA (GA samples) or EPR-g-MA (GB samples) generally increased the physico-mechanical properties including; crosslinking density, tensile strength and thermal degradation resistance etc., when compared with sample without MA or EPR-g-MA (GAO) and the virgin matrix. For the thermal degradation resistance measured by the char residue (%), by using thermal gravimetric analysis technique; GA1 (0.1 ph G and 0.5 ph MA) was 106.4% > XNBR and 58% > GAO (0.1 ph G) while that of GB1 (0.1 ph G and 0.5 ph EPR-g-MA) was 60% > XNBR and 22.2% > GAO respectively. Although, homogeneous dispersions of the G-sheets assisted by MA or EPR-g-MA was a factor, but the strong bonding (covalent, hydrogen and physical entanglements) occurring in GA and GB was observed to be the main contributing factor for these property enhancements. Thus, these nanostructured materials have exhibited multifunctional capabilities and could be used for advanced applications including high temperature (heat sinks), flame retardants, and structural applications.

1. Introduction

The polar and non-polar grades of the elastomeric nanocomposites involving graphene sheets and/or their derivatives (GSD) mostly decorated with oxygenated moieties (C–OH, HO–C=O, OH, C–O–C) have been widely studied for advanced applications in sensors, flexible electronics [1, 2, 3, 4, 5], electromagnetic shields and heat resistance materials [6, 7, 8, 9]. For examples, the single matrix systems such as ethylene propylene-diene monomer (EPDM)-GSD [10, 11], styrene-butadiene rubber (SBR)-GSD [12, 13], acrylonitrile butadiene rubber (NBR)-GSD [6, 14, 15], chlorinated isobutyl isoprene rubber (CIIR)-GSD [16], natural rubber (NR)-GSD [17, 18] and the blend system like; EDPM/silicone-GSD, NR/EPDM-GSD [19], and EPDM/NBR-GSD [20] etc. Some critical issues such as poor dispersion of the GSD into matrices owing to high tendency of the sheets to form agglomerates within the bulk matrix have been reported [21, 22]. GSD are also reported to cause curing delays of elastomer matrices, as they act as scavengers of accelerators [21, 23, 24]. Varghese et al. [25] observed that few layered graphene (FLG) delayed the cross-linking reaction in acrylonitrile rubber. Similar delays in curing of rubber matrices are reported in literature [14, 21, 26, 27]. In addition, the reinforcing mechanism, thermal stability of GSD in elastomer matrix and the poor interfacial interaction between GSD and elastomeric matrices are problems that need to be addressed in elastomer-GDS research [21, 23, 24].

Attempts to address concerns in elastomeric-GSD research has driven research interest in engineering functionalization of the elastomeric matrices and the GSD reinforcements [17, 20, 21, 28]. For example, modification of the chemical structures of elastomers like NR by introduction of epoxide groups along its backbone to form epoxidated natural rubber (ENR) [17, 29] and the conversion of NBR into carboxylated NBR (XNBR) or hydrogenated NBR [30, 31, 32] structures have already been investigated. These tailored matrices are aimed to enhance compatibility of GSD and related fillers, in order to promote strong interfacial interactions, enhance curing and strength to yield a high quality final product [17, 21, 22]. Though, functionalization of GSD via covalent and non-covalent techniques for homogenous dispersion and effective bonding of the individual sheets to a suitable matrix have already been resolved successfully [21, 28, 33, 34, 35]. Several issues still remain, due to complex process steps leading to high cost. A cost-effective and a simple route of preparing polymers composites using traditional fillers like: silica, nanoclays and carbon blacks with suitable coupling agents, which resulted in improved filler dispersions and promoted good

* Corresponding author.
E-mail address: bismarkmensah@ug.edu.gh (B. Mensah).

https://doi.org/10.1016/j.heliyon.2022.e11974
Received 14 April 2022; Received in revised form 11 June 2022; Accepted 22 November 2022

filler-matrix interactions have been explored in the past [36, 37, 38]. Among these processing aids, Maleic anhydride (MA) coupling agent is very popular in preparing these vulcanizates. The MA ($C_2H_2(CO)_2O$) is an organic compound formed by the dehydration of maleic acid [36, 37, 38]. Earlier Lopez et al. [36], successfully used MA as a compatibilizer to improve the interfacial adhesion between hydrophilic flax fibres and hydrophobic polymeric matrices. Chow et al. [37] also observed a significant increase in the mechanical properties in Polyamide (PA6)/Polypropylene (PP)-organoclay composites when ethylene-propylene rubber (EPR)-g-MA compatibilizer was incorporated into the mixture. Recently, Azizli et al. [39] studied the compatibilizer effects of EPDM-g-MA and ENR50 in XNBR/EPDM blend containing different types of nanoparticles (cloisites clays, silica and carbon blacks) and the composites showed improved physico-mechanical properties compared to the ones without compatibilizer or those void of nanoparticles.

The emergence of GSD has also resulted in great research interests in elastomer-GSD composites involving MA [20, 40, 41]. In spite of these efforts, elastomer-GSD research involving MA is still new and more work is needed to be done to address issues relating to the coupling effect in the reinforcing and curing mechanism of GSD in elastomeric matrices, so as to achieve their full potentials for advanced applications.

Earlier, the effects of G and GO in polar NBR and non-polar EPDM matrix were systematically and extensively explored. Weak chemical interactions between GO/G-sheets and rubber matrices was among the findings reported by Mensah et al. [14, 22, 26, 27]. Presently, Mensah's group seeks to study the effect of MA (both pure MA and EPR-g-MA) on the physico-mechanical properties of XNBR in the presence of reduced graphene oxide (G). Various compositions of XNBR-MA-G (GA samples) and XNBR-EPR-g-MA-G (GB samples) were prepared using melt mixing technique. The characterizations include; state of filler dispersions in the matrix, rheological studies by rheometer, crosslinking density analysis, bound rubber test, tensile properties and thermal degradation analysis etc. The results obtained from these tests are clearly presented. Thus, this study gives an insight on how to improve interactions between GSD or related nanoparticles and elastomeric matrix with compatibilizers.

2. Experimental

2.1. Chemicals and compound formulation

The elastomer matrix (carboxylated acrylonitrile-butadiene rubber (XNBR), acrylonitrile content: 20–30 %, carboxylated group: 3–10%) employed in this study was supplied by Kumho Petrochemical Co. Maleic anhydride (MA) crystals (purity 99%, YONGSAN CHEMICALS INC) were supplied by IDONG TECH (South Korea). Reduced graphene oxide (G), with thickness: 0.83–2 nm was synthesized following Hummer's method. Detailed steps for the synthesis and characterizations are already reported in our previous work [27].

The ethylene-propylene-grafted-Maleic anhydride rubber (EPR-g-MA) was supplied by Intelligent Polymer Nano Lab, Polymer Nanotechnology Department, Jonbuk University, South Korea. The rest of the curatives; zinc oxide (ZnO), Stearic acid (SA), Sulfur (S), tetramethyl thiuram disulfide (TMTD), and N-cyclohexile 2-Benzotiazole Sulfonamide (CZ) were all obtained from Infochems Company Ltd (South Korea). The compound formulation expressed as parts per hundred of rubber (phr) with their corresponding codes are listed in Table 1.

2.2. Rubber compounding

The rubber compounding was done using a kneader (model: QPBV-300, QMESYST, South Korea) at 90 °C and 30 rpm. Initially, the rubber was masticated in the kneader for 1 min, with the exception of sulphur; the other processing ingredients were simultaneously added and mixed for about 2 min. The MA or EPR-g-MA was added and mixed for about 1 min. Later, the G-sheets were incorporated and mixed for additional 1 min. The compound was removed and passed over a two-roll mill (QM300, QMESYSTEM) by addition of the sulphur repeatedly for about 10 min and then sheeted out. A rectangular sheet of samples (15 cm × 15 cm x 2 mm) were moulded using electrical hot press machine (model: TO-200, TESTONE. South Korea), at a pressure of 25 tons at 160 °C. The cured composites were allowed to cool overnight and then cut into standard shapes and sizes for characterizations. The tests done include; cure rheology, bound rubber content, crosslinking density studies, tensile properties, and thermal degradation analysis etc.

Table 1. The compound formulation/design expressed in phr.

Chemicals/code	XNBR	GAO	GA1	GA2	GA3	GB1	GB2
XNBR	100	100	100	100	100	100	100
ZnO	5	5	5	5	5	5	5
CZ	0.5	0.5	0.5	0.5	0.5	0.5	0.5
TMTD	0.25	0.25	0.25	0.25	0.25	0.25	0.25
S/A	1.5	1.5	1.5	1.5	1.5	1.5	1.5
Sulfur	2.1	2.1	2.1	2.1	2.1	2.1	2.1
MA	-	0	0.5	0.5	1	-	-
EPR-g-MA	-	-	-	-	-	0.5	0.5
G	-	0.1	0.1	1	0.1	0.1	1

Phr (part per hundred part of rubber), CZ (N-cyclohexyl-2-benzothiazoly-sulfenamide), TMTD (tetramethlythiuram Carbonated nitrile rubber disulphide), S (sulphur), SA (Stearic acid), MAR (Maleic anhydride rubber based), MA (Maleic anhydride) and XNBR (Carbonated nitrile rubber).

3. Characterization

3.1. Particle size distribution of G using DLS

These big-sized G-sheets were weighed 20 mg in falcon tube and 40 ml of distilled water (DW) was added in the tube. The mixture was sonicated for half an hour at room temperature. After the G-sheets were dispersed completely in DW then the resulting mixtures were probe sonicated (power = 450 W, frequency = 20 kHz) for 3 h at 40 % amplitude. Then the solution (probe sonicated for 4 h) was centrifuged at 12 000 rpm, several times (for ~1 h) until no precipitate settled down. The average sheet size for the second solution (4 h probe sonication) was observed as 113 nm. The temperature of the G solution was maintained using an ice bath during sonication.

3.2. Transmission electron microscopy (TEM) analysis of G

A solution of G and dimethyl furan (DMF) were gently dropped on TEM 200-mesh copper grids and allowed to dry. TEM images of the nanoparticles were taken using, JEOL, JEM2100 model.

3.3. Morphological studies by high optical microscopy (HOM)

The structure, state of dispersion and topological information of the XNBR-(G) compositions prepared with the two different MA was observed by using a high optical electron microscopy (HOM) technique obtained from Material Science Lab., University of Ghana. Representative samples of the compositions were cut into dimensions of about 1 cm × 1 cm x 0.1 cm. The results obtained are well discussed.

3.4. Scanning electron microscopy analysis of G and rubber compounds

The morphologies of the G powders were coated with platinum via sputtering and then observed with field emission SEM (JEOL, JSM 599, Japan) obtained from CBNU. Also, the morphologies of the neat XNBR, and the composites (XNBR filled with G-sheets assisted with the different types of the MA and EPR-g-MA) were coated by platinum via sputtering and then observed with field emission SEM.

3.5. Analysis of bound rubber content

Study of bound rubber content in the unvulcanized nanocomposites was done by extracting the unbound rubber in toluene. For the extraction of unbound rubber, ~1.0 g uncured compositions were cut into small size wrapped in cotton bag and immersed in about 300 mL toluene at room temperature for ~7 days. The solution of each composition was changed every two days for 7 days. On the 7th day, the weights of the gel compositions together with the cotton were noted. Later the content in the cotton bag were dried in oven at about 80 °C for ~6 h, air-dried for ~3 and re-weighed. The bound rubber content R_b (%) in each nanocomposite was calculated using Eq. (1) as established in literature [42, 43].

$$R_b(\%) = \left(\frac{W_{fg} - \left[W_t \left(\frac{m_f}{m_f + m_r} \right) \right]}{W_t \left(\frac{m_f}{m_f + m_r} \right)} \right) \times 100 \quad (1)$$

Where, R_b (%) is the content of bound rubber, W_{fg} is the weight of CB and gel, W_t is the weight of nanocomposite. The m_f and m_r are the phr of CB and XNBR rubber in each composition.

3.6. Vulcanization properties of compounds by MDR

The curing properties of the separate vulcanizates prepared with the two different MA in the presence of G within XNBR matrices were studied by using an oscillating-die rheometer (MDR, model: PDR2030, TESTONE. Ltd., South Korea) operating at 160 °C. The various curing parameters including; maximum torque (M_H), minimum torque (M_L), change in torque ($\Delta M = M_H - M_L$), onset of cure time (t_{s2}), optimum cure time (t_{90}), and curing rate index ($CRI = 100/(t_{90}-t_{s2})$) of the various compounds were extracted from the rheo-curves, analysed and presented.

3.7. Crosslinking density by equilibrium swelling test

To estimate the network density of the vulcanizates, representative samples were equilibrated in toluene at room temperature for about 48 h. The swelling degree of he samples was calculated using Eq. (2)

$$Q_r = \frac{W_{sw} - W_i}{W_{dr}} \quad (2)$$

where W_i is the weight of the rubber sample before immersion into solvent, W_{sw} and W_{dr} are the respective weights of the samples in the swollen state and after drying it in oven for about 80 °C for 2 h. Also, the cross-linking density (*N*) was calculated using the Flory-Rehner Eq. (3);

$$\ln(1 - V_2) + V_2 + \chi_1 (V_2)^2 = V_1 N \left[(V_2)^{1/3} - \frac{(V_2)}{2} \right] \quad (3)$$

where V_2 is the volume fraction of polymer in the swollen gel at equilibrium, V_1 is the molar volume of the for toluene used (106.3 mL/mol) and χ_1 (0.374) is the polymer-solvent parameter determined from Bristow-Watson Eq. (4) [44].

$$\chi_1 = \beta_1 + \left(\frac{V_1}{RT} \right) (\delta_s - \delta_p)^2 \quad (4)$$

where β is the lattice constant, usually taken as 0.34, V_1 is the molar volume of solvent (106.3 mL/mol), R is the universal gas constant, T is the absolute temperature and δ is the solubility parameter for the solvent (s) and polymer matrix (p) respectively. The solubility parameters of elastomer and the solvent toluene were 8.4 and 9.29 $(cal/cc)^{1/2}$ [45] respectively.

3.8. Tensile test

The tensile properties measurement was done for the vulcanizates based on ASTM D412 standard by using (QM100s machine, QMESYSTEM, South Korea) at a cross-head speed of 500 mm/min and at 25 °C temperatures. Three samples were tested for each composition and averaged.

3.9. Thermal gravimetric analysis (TGA)

TGA was done to test for the thermal degradation resistance behaviour of the representative samples of XNBR, GAO, GA and GB, using a SDT Q600-TA. The conditions used for this test include; a nitrogen medium, equilibrium temperature of ~25 °C and a heating rate of 10 °C/min to a maximum temperature of 800 °C.

4. Results and discussion

4.1. Morphology, structure and particle size of G-sheets

Detailed characterizations of graphene oxide (GO) and G using Fourier transform infrared spectroscopy, Wide-angle x-ray diffraction (WAXD), Raman, and UV-spectra, have been reported in our previous work [22, 26]. For the purpose of this current work, we present an SEM, TEM and a DLS analysis of the prepared G-sheets, as shown in Figure 1(a-c) respectively.

The extensive oxidation, exfoliation and further reduction of GO into G-sheets by hydrazine leaves the nanostructured materials amorphous with imperfections, characterized with wrinkled sheets by the SEM image in Figure 1a. The TEM image in Figure 1b also shows a similar structural deformation of wrinkled and folded transparent sheets. These amorphous and wrinkled structures occurs for the 2D-nanomaterial to attain thermodynamic stability [27] whilst it may offer advantages in confining and restricting the mobility of the polymer chains thereby improving the physico-mechanical properties of the resulting composites [21, 46]. By using the TEM scale bar, G-sheets show an estimated thickness between 0.83-2 nm. Also, Figure 1c demonstrates the particle size distribution of G-sheets measured by the DLS. As shown in Figure 1c, the hydrodynamic diameter of G sheets is about 113 nm. The *G nanoparticles* were generally observed to be suitable as reinforcements to form composite with XBNR matrix for further studies.

4.2. Morphology and state of dispersion of fillers

To understand the state of dispersions of G-sheets within the XNBR matrix in the presence of MA or EPR-g-MA, high optical microscopy (HOM) and SEM techniques were used as shown in Figure 2(a-h). Figure 2(a-d) represent HOM images of the virgin XNBR, GAO, GA1 and GB1. The XNBR (Figure 2a) shows a very smooth surface while the composites (Figure 2(b-d)) show rough and non-uniform surface. The dark phase regions are dispersed G-sheets in XNBR matrix, with particle size ranging from few nanometer to above 100 μm.

To further evaluate the dispersion of G sheets in XNBR composites, SEM images of XNBR, GAO, GA1 and GB1 are depicted in Figure 2(e-h). It can be seen that cryo-fractured XNBR matrix shows a smooth surface structure. From Figure 2f-h, the fractured surfaces become rough and uneven due to G sheets added. The presence and the strong bonding of MA or EPR-g-MA in the presence of the G-sheets with XNBR, makes it difficult to break pieces of these representative samples by cryogenic fracturing process for SEM observation. This difficulty induces rough futures at the observing surfaces. Such rough morphological nature of rubber composites is reported to be an indication for effective load transfer at the filler-rubber matrix interfaces, leading to improvement in mechanical properties [47, 48, 49]. It is seen that there are no observable agglomerates across the whole XNBR surface and this indicates a good dispersion and distribution of G-sheets within the XNBR matrix.

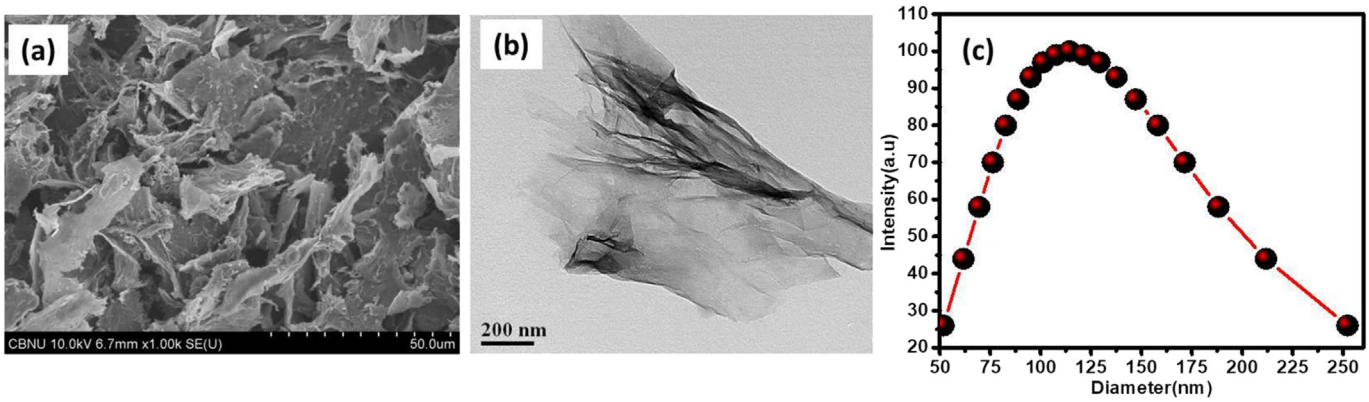

Figure 1. Morphology, structure and particle size of G-sheets: (a) SEM (b) TEM and (c) DLS.

4.3. Vulcanization properties

4.3.1. Vulcanization mechanism

The on-set of cure and optimum curing time (t_{s2}, and T_{90}) and the cure rate index (CRI) of the various samples are compared in Figure 3(a-c) respectively. Clearly, the virgin matrix (XNBR) showed the fastest t_{s2} when compared to the remaining samples. The GAO sample experienced a slight delay in t_{s2} due to the incorporation of the G-sheets. Delays in t_{s2} may be due to the increase in initial viscosity of the compounds, which delays melting of the curatives to start crosslinking reaction [50]. Upon addition of MA or EPR-g-MA in the presence of the G-sheets, the t_{s2} values increased further for the corresponding samples when compared with the XNBR and the GAO. Azizli et. al [51]. recently observed that increasing the content of GO in silicone rubber (PVMQ)/XNBR blend in the presence of XNBR-g-GMA as a compatibilizer decreased the scorch time (t_{s2}) by 24 %. Clearly, there are inconsistent reports on the reasons for delays in scorch time (t_{s2}) for rubber vulcanizates, which may be as a result of different factors like; type of matrix, filler, processing aids and conditions used. However delays in t_{s2} may be useful as it may allow enough time for both the matrix and vulcanization ingredients to melt in order to ensure a stable crosslinking reactions to yield desired final products [22, 26, 50].

The T_{90} and CRI in Figure 3(b and c) for the pure matrix (XNBR) outperformed that of the composites. Thus, it can be speculated that faster curing reactions ($t_{s2,}$ T_{90} and CRI) for XNBR could be linked to the presence of fewer interactions which include; the physical polar-polar chain entanglements (XNBR-XNBR) and the main chain or primary crosslinking reactions between the unsaturated groups (C=C) of XNBR and the monomeric polysulfide structures (Bt-S-S_x-S-Bt). These Bt-S-S_x-S-Bt structures are formed by the curatives; sulphur (S), accelerator and activators [14]. The Bt is an organic radical that is derived from the accelerator (benzothiazyl) during the crosslinking reaction [50, 52]. Also, the reason for faster curing of XNBR is due to the absence of G, which is reported to be scavengers for curing aids [25]. When compared, G-sheets delayed the crosslinking reaction of GA1-GA3 more than those of GB1 and GB2. This could be explained in terms of the high melting point of MA, higher number of interactions (mostly polar-polar interactions) and higher bulk viscosity of GA nanocomposites.

During the vulcanization process, the pure MA salts with its high melting point requires enough time to melt before engaging in crosslinking reactions. Also, MA and G-sheets react through grafting (MA-g-G) and later grafted to the main chain (XNBR-g-G-MA-g-G-XNBR) other interactions like; hydrogen bonding (polar-polar interactions) between the nitrile groups of XNBR and OH of G ($C{\equiv}N^{\delta-}{-}H^{\delta+}{-}O$), physical entanglement of the polar-polar chains of XNBR (XNBR-XNBR) and the reaction between the carboxylic groups (HO–C=O) of XNBR and those decorating the G-sheets etc. are all possible [14, 27]. These interactions are as illustrated in Figure 4(a&b). The contribution from these secondary interactions in addition to the primary crosslinking reactions of the main chain (XNBR-S-S_x-XNBR) could be the main reason for the delays seen in their curing times (t_{s2} and T_{90}) and the CRI (Figure 3c.) when

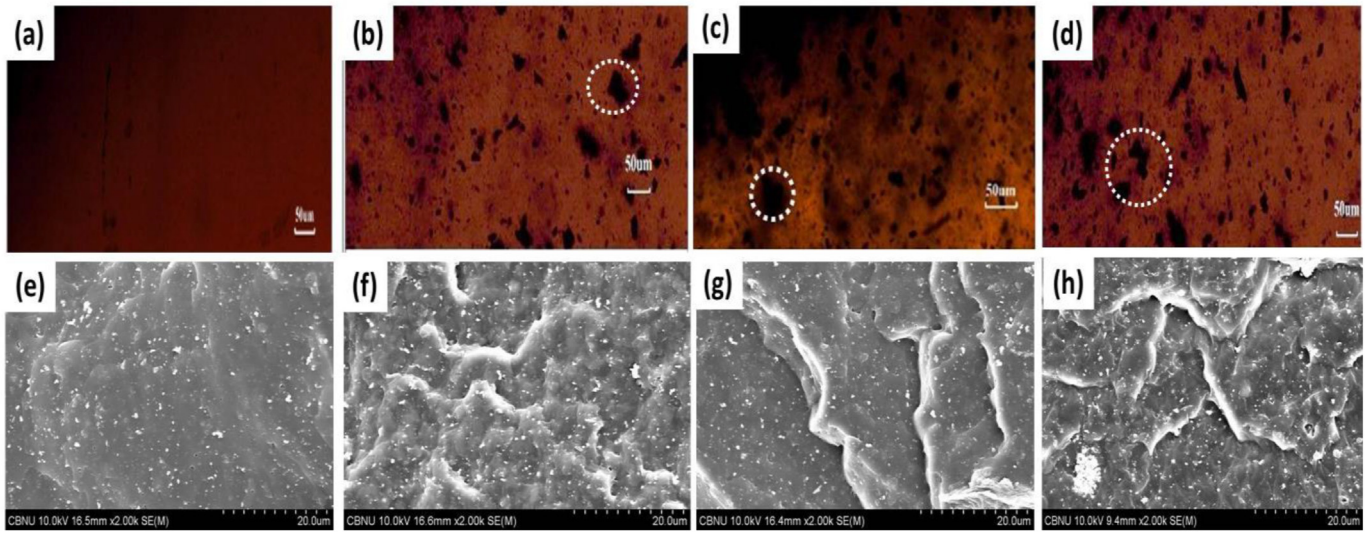

Figure 2. Morphological properties of the cross-sections of the representative samples by HOM: (a) XNBR, (b) GAO, (c) GA1 (d) GB1 and by SEM: (e) XNBR, (f) GAO, (g) GA1 and (h) GB1.

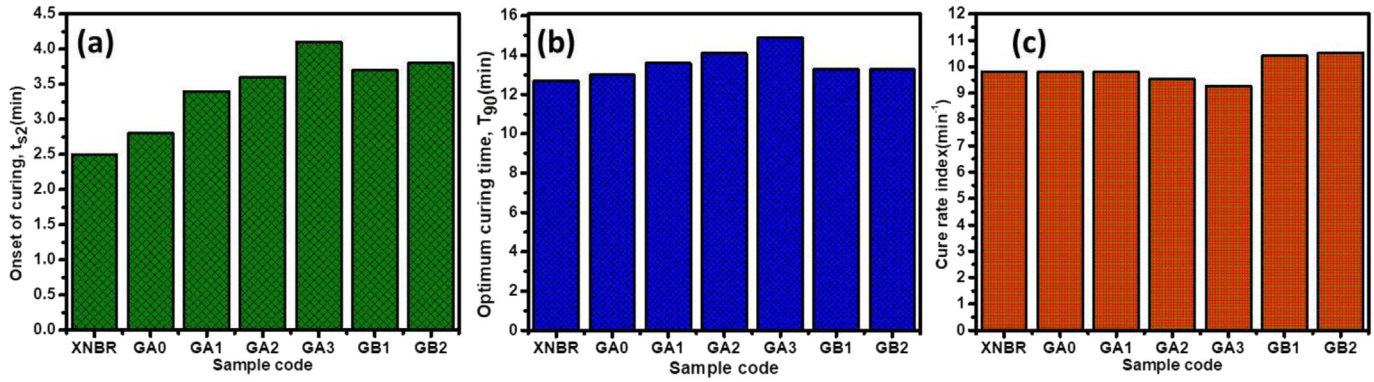

Figure 3. Cure properties: (a) scorch time (t_{s2}) (b) optimum curing time (T_{90}) and (c) Cure rate index (CRI).

compared with GB vulcanizates. This observation contradicts the idea that graphene sheets act as scavengers of cure accelerators [25]. Meanwhile, an advantage of these numerous interactions is the creation of tight network structures with high viscosities. Similarly, as depicted in Figure 5(a&b), many interactions: both primary and secondary are all possible in GB vulcanizates, however on heating, EPR-g-MA as rubber may exhibit relatively faster melting behaviour (low viscosity) to engage in crosslinking process reactions than the counterpart MA.

Besides, interactions in GB vulcanizates generally include a mixture of polar interactions such as XNBR-S-S_x-XNBR and $C{\equiv}N^{\delta-}{-}H^{\delta+}{-}O$, physical chain entanglements among the polar matrix (XNBR-XNBR) and chain entanglements among the saturated (C–C) non-polar matrix (EPR-EPR and EP-g-MA-EPR). There may also be physical and chemical interactions among their blends: polar-non-polar interactions (EPR-g-MA-g-G-XNBR) and their physical chain entanglements (EPR-XNBR). These heterogeneous interactions (mainly physical) within the GB nanocomposites may not promote effective tighter structures associated with high viscosities as compared to those in GA samples. Hence, it was easy for crosslinking reaction to ensue consequently in GB samples. This could account for their faster crosslinking reaction times (t_{s2} and T_{90}) and cure rate index (CRI). It was observed that EPR-g-MA is best additive for promoting faster curing of XNBR matrix, especially in the presence of G-sheets as compared to the pure MA [41, 53].

4.3.2. *Curing viscosity, density mechanical strength index*

The effects of MA, EPR-g-MA and G-sheets on the minimum torque or viscosity index (M_L) of XNBR are compared in Figure 6(a). Addition of 0.1 ph G-sheets into XNBR (GAO sample) shot up the M_L to a value above 7 % higher than the pure XNBR. Meanwhile, when MA was added, further increment of M_L above 41 % for samples GA1 and 44 % for GA2 were recorded when compared with pure matrix XNBR as well as 58 % and 55 % higher M_L in comparison with those containing EPR-g-MA (GB1

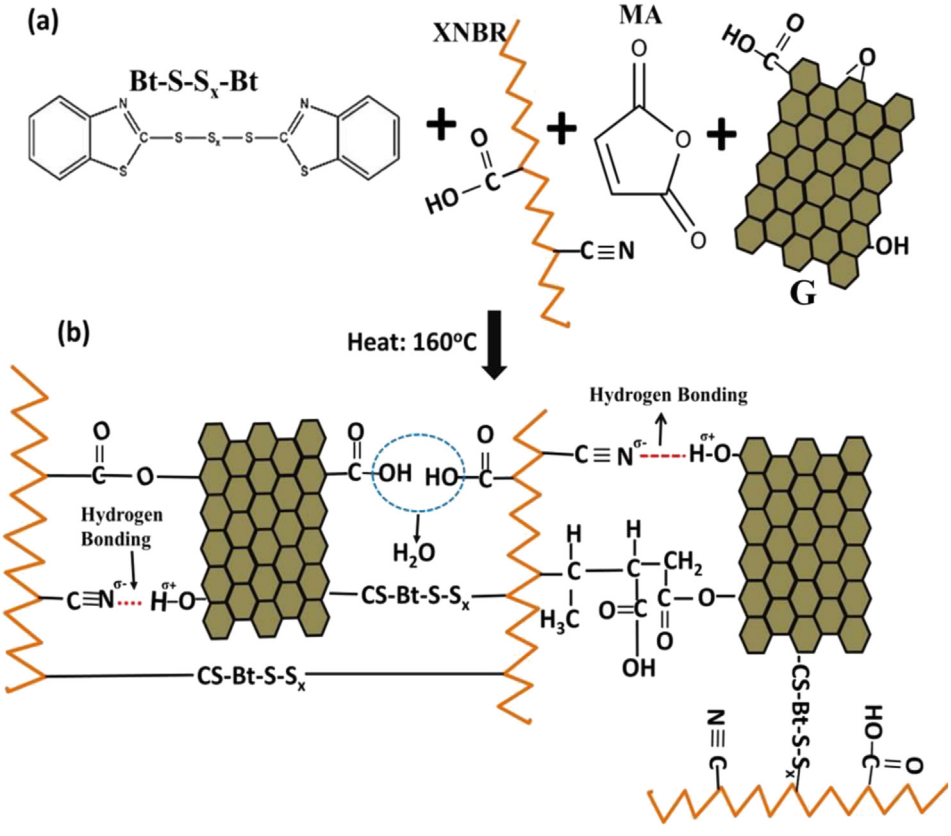

Figure 4. A depiction of the crosslinking reaction mechanism of polysulfidic species, XNBR, pure MA salt and G-sheets.

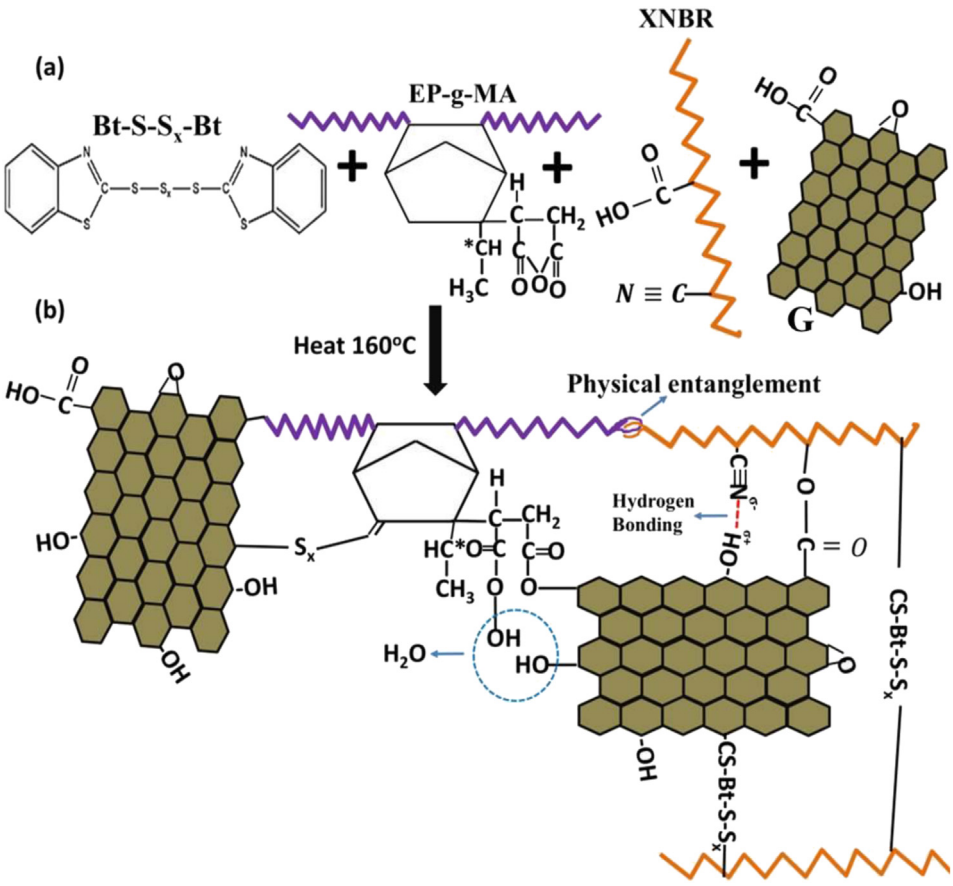

Figure 5. A depiction of reaction mechanism of polysulfidic species, XNBR, EPR-g-MA, and G-sheets.

and GB2 samples). The increase in M_L can be linked to viscosity to numerous interactions (higher crosslinking density effect), restricting the mobility of the XNBR chains [22, 26, 50]. Interestingly, at higher MA loading of 1 ph (GA3 sample), the M_L declined for GA3 and this could be an indication of over-curing resulting in degradation of the networked structures [54]. The high viscosity index (M_L) results justify the slow curing nature as observed for GA vulcanizates.

The crosslinking density and mechanical strength indicators (M_H, and ΔM) of the vulcanizates are compared in Figure 6(b) and Figure 6(c). The polar nature of XNBR is known to promote effective crosslinking reaction, adding the G-sheets and MA significantly increases the total network densities. This might have resulted in over curing reversion where network begins to break as earlier observed in ENR-SBR containing 3 ph of MA [55]. An opposite trend can be seen when MA was substituted with EPR-g-MA, that is, an increase in the EPR-g-MA tends to increase the (M_H, and ΔM) slightly, even so these properties were comparable to XNBR and GAO compounds. It should be noted that, torque values (M_L, M_H, and ΔM) generated from cure rheometry depends on several factors including; the processing, conditions, filler-filler, polymer-filler networks and chain-chain interactions [56, 57]. However, desired networks structures can generally boost the physico-mechanical properties of rubber composite [21, 26]. To understand the reinforcing mechanisms that caused the differences in the values of (M_L, M_H and $\Delta M = M_H$-M_L) for both MA and EPR-g-MA compositions, further analysis like; bound rubber and chemical crosslinking density by equilibrium swelling are carefully examined and reported.

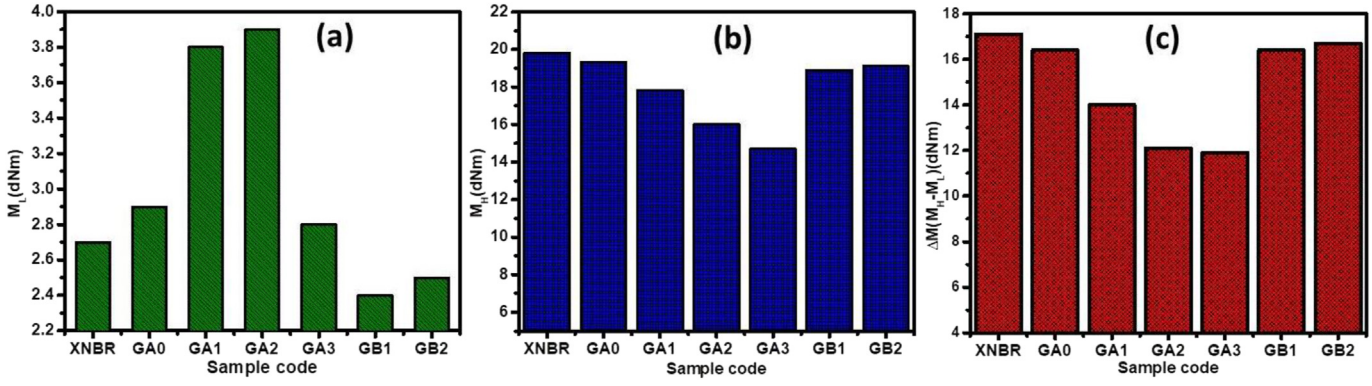

Figure 6. Cure properties: (a) viscosity index (M_L) (t_{s2}) (b) network density index (M_H) and (c) mechanical strength index ($\Delta M = M_H$-M_L).

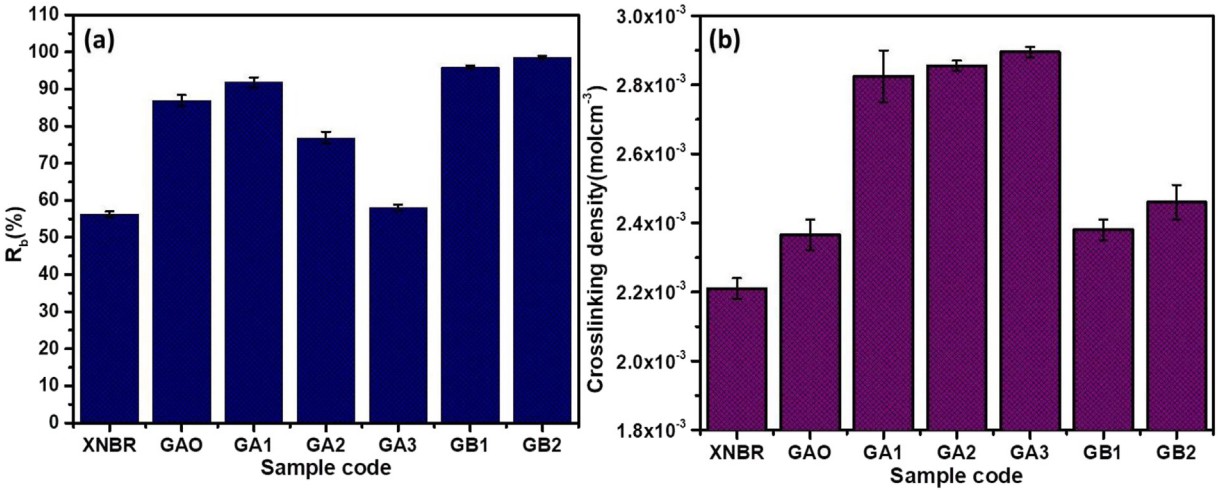

Figure 7. Filler-polymer chain interactions indicators (a) Bound rubber content, R_b (%) and (b) Chemical crosslinking density (molcm^{-3}).

4.4. Bound rubber content and crosslinking density

Rubber bound content helps to understand the initial formation of network structure (gel) in nanocomposite. The bound rubber content R_b (%) practically depends on rubber-filler interactions in uncured state of composites [14]. The bound rubbers for the various compositions (filled and unfilled) are showed in Figure 7a. The R_b (%) for the gum was significantly lowered due to the absence of G-sheets or coupler (MA or EPR-g-MA) but on addition of the G-sheets (GAO sample) it rose above 50% relative to XNBR. In the presence of MA or EPR-g-MA and G-sheets, a general increment in Rb (%) was observed from GA1 to G3 and GB1 to GB2 in comparison with pure XNBR. This increment may due to the

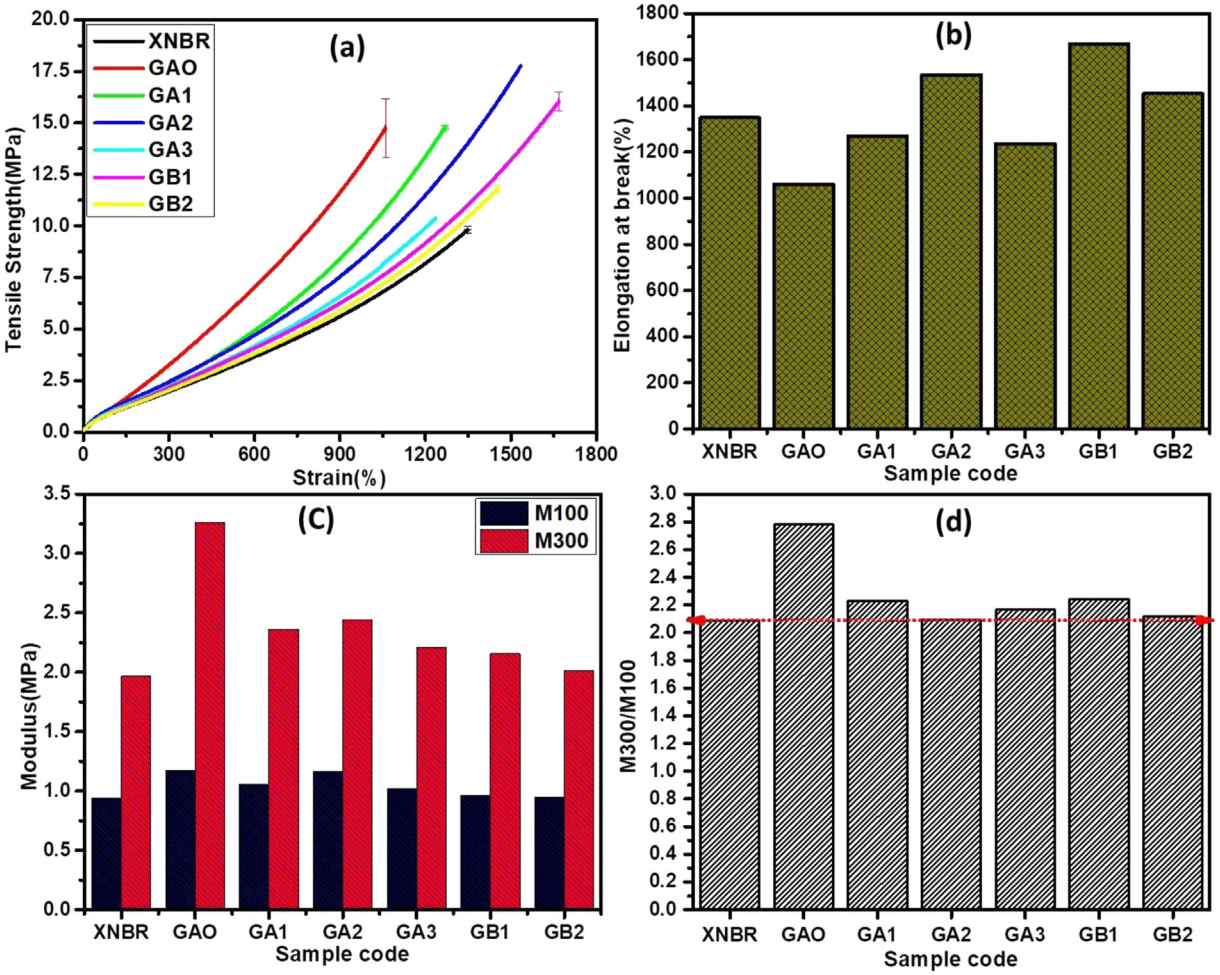

Figure 8. Tensile properties of vulcanizates: (a) Stress-strain curve (b) elongation at break (%) (c) Modulus at 100% strain (M100) and 300% strain (M300) and (d) Reinforcement factor (M300/M100).

strong interactions like hydrogen bonding in XNBR-G assisted by MA or EPR-g-MA [20, 51, 58]. However, the GB samples seem to show slight increment in R_b (%) than its counterparts (GA1-GA3). In their uncured state, GB samples (dual matrix phase of EPR and XNBR chains) could have high tendency to physically entrap or adhere to the G-sheets and the curatives within their structures strongly than the GA (one matrix system) samples.

After vulcanization, it was clear that when MA was added to the G-sheets mixture, crosslinking density, *N* ($molcm^{-3}$) values increased significantly compared to composites containing the EPR-g-MA as shown in Figure 7b. Two mechanisms are known for an increment in *N;* better dispersion of fillers within the matrix, and/or the strong interfacial interactions of filler-matrix [22, 26, 50]. Here, the numerous nd effective filler-G sheets bonding assisted by the MA were responsible for high *N* ($molcm^{-3}$) in GA samples than those of GB which were observed to be mostly physical interactions. This is as depicted earlier in Figure 4(a&b) and Figure 5(a & b) respectively. Earlier, G and GO exhibited higher network structures in polar NBR than the non-polar EPDM counterparts [26]. The *N* ($molcm^{-3}$) test has confirmed that incorporation of G-sheets into XNBR in presence of MA or EPR-g-MA generally enhance dispersions of G-sheets and also improves the interfacial interactions between XNBR and the G-sheets.

4.5. Tensile properties

Tensile strength properties of composites mainly depend on some factors: (i) surface chemistry of G sheets, (ii) grafting efficiency of MA or EPR-g-MA, (iii) interfacial interactions between G sheets and XNBR chains (like; XNBR-S_x-G-g-MA-g-XNBR, XNBR-G, and XNBR-S_x-EPR-g-MA-g-G), and (iv) several other interactions among individual G sheets (like; G-S_x-G or G-G) [20, 51, 58]. Figure 8(a-d), shows the tensile properties of XNBR and its nanocomposites. Generally, addition of the G-sheets into the XNBR matrix improved the tensile strength compared to the virgin matrix. However, when MA was incorporated, the strength was seen increasing further for GA1 and GA2 until it declined at GA3 (1 ph MA). At this high loading level of MA, it was suspected that extreme network density was created in GA3 matrix which reduced its viscoelasticity, thereby making it brittle-like and easy to fracture. The result was the lower tensile strength recorded.

It is seen that the GA2 (1 ph G and 0.5 ph MA) composite exhibits the highest tensile strength, signifying it contained desired amount of network structures enough to transfer stress across the interface of G-sheets and the matrix [21, 23, 48]. When compared, the GB1 had over 8% growth in tensile strength than its counterpart GA1. Meanwhile, GA2 also attained over 52% strength compared to GB2. Therefore, GA samples have generally indicated higher tensile strength than those of GB samples. On the other hand, the GB samples seem to have broadly exhibited higher elongation at break (%) behaviour compared to GA samples, significantly at low G-sheets (0.1 ph)-loading level (Figure 8b). For example; while the GA2 had about 6% increment in elongation at break (%) than their counterparts GB1, the GB1 obtained ~31% elongation at break (%) than GA1. This increment may predominantly be due to weaker filler-matrix interactions (physical interactions) with high mobility and lower stiffness of the chains rather than chemical links

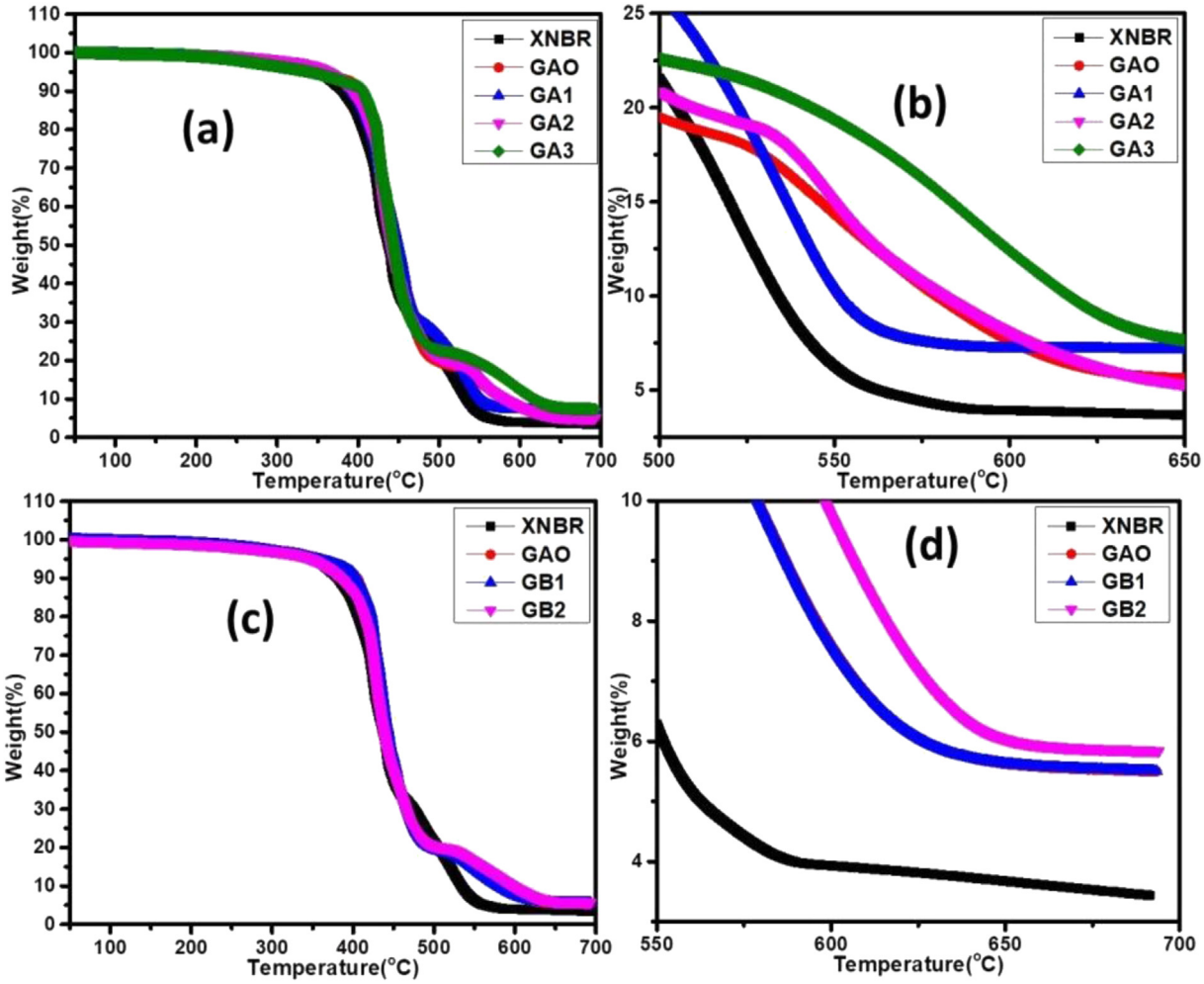

Figure 9. TGA curves for XNBR-G assisted MA and EPR-g-MA samples (a) GA samples (b) exaggerated curves for GA samples(c) GB samples and (c) exaggerated curves for GB samples.

Table 2. TGA results of current research and other related work rubber-*G nanocomposites*

Composition/code	Percentage increase in Residue (%) with reference to pure matrix	T_i (°C)	T_{max} (°C)	Remarks
XNBR	3.44	382	534	Current work
GAO (0.1 ph G)	4.50 (31% > XNBR)	391	601	-
GA1 (0.1 ph G, 0.5 ph MA)	7.1 (106.4% > XNBR and 58% > GAO)	394	552	-
GA2 (1 ph G, 0.5 ph MA)	5.01 (46% > XNBR and 11.3% > GAO)	392	582	-
GA3 (0.1 ph G, 1 ph MA)	7.3 (112.2% > XNBR and 62.2% > GAO)	406	617	-
GB1 (0.1 ph G, 0.5 ph RMA)	5.5 (60% > XNBR and 22.2% > GAO)	405	579	-
GB2 (1 ph G, 0.5 ph RMA)	5.6 (63% > XNBR and 24.4% > GAO)	384	598	-
BIIR* (4wt% GO-IL)	-	-	405	2013 [60]
NBR (1 ph GO)**	9.4/7.8 (21% > NBR)			2014 [22]
SBR (7 ph G)	~10/6 (67% > SBR)	-	-	2014 [61]
XNBR (2 ph GO-HDA)***	~6.5/4 (63% > XNBR)	394	-	2016 [62]
NR (1.1 ph of G)	~12/8 (50% > NR)	352.5	460.5	2020 [63]

*GO functionalized ionic liquid in bromo-isoprene isobutylene rubber (BIIR), **NBR: author's previous work, and ***GO functionalized with hexadecyl amine (HDA).

(Figure 7c). On computing the reinforcing factor (M300/M100), as shown Figure 7d, it was interesting to see the GAO exhibited the highest M300/M100 property, which may mostly be related to high physical interactions (G-S_x-G or G-$O^{\delta-}$—H $^{\delta+}$-G) within GAO. These weak interactions were easily broken at higher strain by Payne's effect [59], hence the lower ultimate tensile strength (UTS) recorded, as compared to the compounds with high UTS (GA1, GA2 and GB1) whose reinforcing mechanism were mainly controlled by chemical networks. Clearly, the addition of MA or EPR-g-MA in presence of G-sheets benefited the pure matrix by enhancing its filler-matrix networks for GA and GB samples. Therefore, this current work presents samples with improved tensile properties compared to matrices filled with even higher content or functionalized GDS as summarised in the following rubber-GDS review works [21, 23].

4.6. Thermal degradation properties

The weight residue (%) as a function of temperature for XNBR, GAO and GA and GB compositions has been presented in Figure 9(a-d). Figure 9(b&d) respectively are presented for clarity. The weight residues (%) and the respective temperature for decomposition (T_i and T_{max}) which represents initial (10 % degradation) and maximum decomposition (90 % of degradation) of the composition was used to characterize the extent of thermal degradation of the various compounds as summarised in Table 2. In Figure 9a (Figure 9b for clarity) and Figure 9c (clearly shown in Figure 9d), the GA and GB samples broadly seemed to shield the XNBR matrix effectively from decomposition, this was associated with higher weight residue (%) when compared with the neat XNBR and the GAO. It was interesting to observe that higher content of the maleic anhydrides further increases the weight residues (%) for the composition (see the case of GA3); however increasing the content of the G-sheets did not have the same effect (see samples GA2 and GB2) in Table 2. In Table 2, a trend can be observed; degradation shifts from lower (T_i) to higher temperatures (T_{max}). The minimum and maximum decomposition of the XNBR occurred at 382 and 532 °C respectively and upon addition of G-sheets or MA and EPR-g-MA, the T_i and T_{max} for GAO, GA and GB samples increased. Thus, higher heat was used to decompose these samples compared to XNBR.

Although, some scattered data can be observed in the weight residue (%), T_i and T_{max} for the filled compositions, however GA samples generally showed higher decomposition resistance compared to the GB. The much tighter structures associated with higher crosslinking density, N (molcm^{-3}) and viscosity contained in GA samples introduced by MA-g-G-sheets might be the controlling factor for this enhancement. The current results outperformed those obtained in our previous work [22] contained in Table 2 where NBR was reinforced with 1 ph of GO in the absence of MA or EPR-g-MA. Also, the current results outperform the thermal degradation resistance of rubber-GDS composites already reported by other researchers [60, 62, 64], as presented in Table 2. It can therefore be concluded that, in this current work, it seems the combined effect of the physical presence of the G-sheets, their enhanced dispersions and particularly their grafting to the XNBR matrix by MA or EPR-g-MA, creating numerous tight networks structures, might be the controlling factors for the thermal degradation resistance property enhancement. Thus, the matrix was protected by the combined effect of these factors by delaying the leakage of pyrolysis products to cause further degradation of the main matrix [21, 22].

5. Conclusion

Nanoparticles of reduced graphene oxide (G) assisted by two different kinds of maleic-anhydrides: ethylene-propylene grafted-maleic anhydride (EPR-g-MA) and a pure maleic anhydride (MA)) was used to reinforce carboxylated acrylonitrile butadiene-rubber (XNBR) to form nanocomposites by using melt compounding technique. It was observed that MA in presence of G-sheets delayed the curing of XNBR (GA samples) than XNBR containing EP-g-MA (GB samples), supposedly due to high melting behaviour of the MA and the tighter network structures created in the matrices. The tighter structures in GA nanocomposites was due to the combination of chemical interactions (XNBR-g-G-MA-XNBR and XNBR-S-S_x-XNBR) and physical interactions (C≡$N^{\delta-}$—$H^{\delta+}$—O and XNBR-XNBR) whilst those in GB nanocomposites were observed to be mainly mixtures of polar and non-polar (XNBR-g-G-EPR-g-MA) interactions. The EPR-g-MA is rubber containing MA grafted to EPR matrix; hence chain mobility in EPR-g-MA could occur quickly above glass transition temperatures for both primary and secondary crosslinking reactions ensue. This was the reasons for the slow crosslinking reactions (longer t_{s2} and T_{90}) of the GA samples than their counterparts (GB samples). Consequently, the tighter network structures in GA resulted in higher crosslinking density, N (molcm^{-3}), higher viscosity index (M_L), strength and modulus than GB samples. It was interesting to observe that GB samples obtained higher elongation at break (%) than the GA samples noted for high ductility, as results of the physical entanglement between EPR-g-MA and XNBR. In terms of thermal degradation study by TGA, the GA samples outperformed the GB samples the differences in the char residue (%) is considered. The sample GA1 (0.1 ph G-sheets and 0.5 ph MA) exhibited higher weight residue (%) of 106.4% > XNBR and 58% > GAO (0.1 ph G-sheets). However, its counterpart GB1 (0.1 ph G-sheets and 0.5 EP R-g-MA) was 60% > XNBR and 22.2% > GAO respectively. In summary, the presence of MA or EPR-g-MA in the presence of G-sheets improved the physico-mechanical properties of the currently prepared samples (GAO and XNBR) including those already reported by other researchers. Therefore, the present work has demonstrated a simple way of enhancing physico-mechanical properties of rubber matrix by controlling

its microstructure with G-sheets assisted with suitable coupler like Maleic anhydride (MA or EPR-g-MA). Such nanocomposites materials could have multifunctional capabilities such as high temperature applications (heat sinks), flame retardants, and structural materials upon further optimization etc.

Declarations

Author contribution statement

Bismark Mensah: Conceived and designed the experiments; Performed the experiments; Analyzed and interpreted the data; Contributed reagents, materials, analysis tools or data; Wrote the paper.

Johnson Kwame Efavi, David Sasu Konadu: Analyzed and interpreted the data.

Gloria Pokuaa Manu: Performed the experiments.

Funding statement

This research did not receive any specific grant from funding agencies in the public, commercial, or not-for-profit sectors.

Data availability statement

Data will be made available on request.

Declaration of interests statement

The authors declare no competing interests.

Additional information

No additional information is available for this paper.

Acknowledgements

We thankfully acknowledge the support from Professor Changwoon Nah (Intelligent Polymer Nano-materials Lab) of Polymer Nano-science and Technology Department, Jeonbuk National University, for supplying us materials for our studies. We thankfully acknowledge Yuntech Co. Ltd (South Korea) for allowing us to use their facility to carry out this study. We also acknowledge the Office of Research, Innovation and Development (ORID) of University of Ghana for making this study successful.

References

[1] S.-H. Bae, et al., Graphene-based transparent strain sensor, Carbon 51 (2013) 236–242.
[2] C.S. Boland, et al., Sensitive, high-strain, high-rate bodily motion sensors based on graphene-rubber composites, ACS Nano 8 (9) (2014) 8819–8830.
[3] X. You, J.J. Pak, Graphene-based field effect transistor enzymatic glucose biosensor using silk protein for enzyme immobilization and device substrate, Sensor. Actuator. B Chem. 202 (2014) 1357–1365.
[4] T. Kuila, et al., Recent advances in graphene-based biosensors, Biosens. Bioelectron. 26 (12) (2011) 4637–4648.
[5] T.T. Tung, et al., Engineering of graphene/epoxy nanocomposites with improved distribution of graphene nanosheets for advanced piezo-resistive mechanical sensing, J. Mater. Chem. C 4 (16) (2016) 3422–3430.
[6] Zheng, et al. Development and application of electromagnetic shielding material with silicone rubber graphene structure 774, IOP Conf. Ser. Mater. Sci. Eng., 2020, 012131.
[7] W. Chen, L. Yan, Preparation of graphene by a low-temperature thermal reduction at atmosphere pressure, Nanoscale 2 (4) (2010) 559–563.
[8] Li, et al., Thermally conductive and antistatic properties of silicone rubber reinforced by the modified graphene oxide, Polymers 14 (2022) 1421–4703.
[9] L. Gan, et al., Facile preparation of graphene nanoribbon filled silicone rubber nanocomposite with improved thermal and mechanical properties, Compos. B Eng. 69 (2015) 237–242.
[10] A. Allahbakhsh, et al., Cure kinetics and chemorheology of EPDM/graphene oxide nanocomposites, Thermochim. Acta 563 (2013) 22–32.
[11] L. Valentini, et al., Pyroshock testing on graphene based EPDM nanocomposites, Compos. B Eng. 60 (2014) 479–484.
[12] S. Schopp, et al., Functionalized graphene and carbon materials as components of styrene-butadiene rubber nanocomposites prepared by aqueous dispersion blending, Macromol. Mater. Eng. 299 (3) (2014) 319–329.
[13] Z. Tang, et al., Preparation of butadiene-styrene-vinyl pyridine rubber-graphene oxide hybrids through co-coagulation process and in situ interface tailoring, J. Mater. Chem. 22 (15) (2012) 7492–7501.
[14] B. Mensah, et al., A comparative study on vulcanization behavior of acrylonitrile-butadiene rubber reinforced with graphene oxide and reduced graphene oxide as fillers, Polym. Test. 76 (January) (2019) 127–137.
[15] B. Mensah, et al., Gold Functionalized-Graphene Oxide-Reinforced Acrylonitrile Butadiene Rubber Nanocomposites for Piezoresistive and Piezoelectric Applications, 2018.
[16] D. Frasca, et al., Multilayer graphene/carbon black/chlorine isobutyl isoprene rubber nanocomposites, Polymers 8 (3) (2016) 95.
[17] K. Ka Wei, et al., Enhancing compatibility in epoxy/vulcanized natural rubber (VNR)/Graphene nano-platelets (GNP) system using epoxidized natural rubber (ENR-50), Compos. B Eng. 174 (2019), 107058.
[18] H. Kang, et al., Fabrication of graphene/natural rubber nanocomposites with high dynamic properties through convenient mechanical mixing, Compos. B Eng. 112 (2017) 1–7.
[19] J. Abd Razak, in: S. Haji Ahmad, et al. (Eds.), Graphene Nanoplatelets-Filled NR/EPDM Rubber Blend: Effects of GNPs Loading on Blend Processability, Mechanical Properties and Fracture Morphology, Nova Science Publishers, Inc., 2015.
[20] M.J. Azizli, et al., Compatibilizer/graphene/carboxylated acrylonitrile butadiene rubber (XNBR)/ethylenepropylenediene monomer (EPDM) nanocomposites: morphology, compatibility, rheology and mechanical properties, J. Appl. Polym. Sci. 137 (43) (2020) app49331.
[21] B. Mensah, et al., Graphene-reinforced elastomeric nanocomposites: a review, Polym. Test. 68 (2018) 160–184.
[22] B. Mensah, et al., A study of graphene oxide-reinforced rubber nanocomposite, J. Appl. Polym. Sci. 131 (16) (2014).
[23] X. Liu, et al., Research progress of graphene-based rubber nanocomposites, Polym. Compos. 39 (2016) 1006–1022.
[24] Y. Li, et al., Preparation and tribological properties of graphene oxide/nitrile rubber nanocomposites, J. Mater. Sci. 47 (2) (2012) 730–738.
[25] T.V. Varghese, et al., Reinforcement of acrylonitrile butadiene rubber using pristine few layer graphene and its hybrid fillers, Carbon 61 (2013) 476–486.
[26] B. Mensah, et al., Effect of graphene on polar and nonpolar rubber matrices, Mechanics of Advanced Materials and Modern Processes 4 (1) (2018) 1.
[27] B. Mensah, et al., Preparation and properties of acrylonitrile–butadiene rubber–graphene nanocomposites, J. Appl. Polym. Sci. 132 (36) (2015) 1097–4628.
[28] D.R. Dreyer, et al., The chemistry of graphene oxide, Chem. Soc. Rev. 39 (1) (2010) 228–240.
[29] S. Yaragalla, et al., Effect of reinforcement on the barrier and dielectric properties of epoxidized natural rubber–graphene nanocomposites, Polym. Eng. Sci. 55 (11) (2015) 2439–2447.
[30] M. Mirzaei Aliabadi, et al., Transport properties of carboxylated nitrile butadiene rubber (XNBR)-nanoclay composites; a promising material for protective gloves in occupational exposures, J Environ Health Sci Eng 12 (1) (2014) 51.
[31] I. Smaoui, et al., Eco-friendly nanocomposites between carboxylated acrylonitrile–butadiene rubber (XNBR) and graphene oxide or graphene at low content with enhanced mechanical properties, Fullerenes, Nanotub. Carbon Nanostruct. 24 (12) (2016) 769–778.
[32] M. Tian, et al., High performance dielectric composites by latex compounding of graphene oxide-encapsulated carbon nanosphere hybrids with XNBR, J. Mater. Chem. 2 (29) (2014) 11144–11154.
[33] K. Haubner, et al., The route to functional graphene oxide, ChemPhysChem 11 (10) (2010) 2131–2139.
[34] H. Kim, A.A. Abdala, C.W. Macosko, Graphene/polymer nanocomposites, Macromolecules 43 (16) (2010) 6515–6530.
[35] T. Kuila, et al., Chemical functionalization of graphene and its applications, Prog. Mater. Sci. 57 (7) (2012) 1061–1105.
[36] P. Kueseng, P. Sae-oui, N. Rattanasom, Mechanical and electrical properties of natural rubber and nitrile rubber blends filled with multi-wall carbon nanotube: effect of preparation methods, Polym. Test. 32 (4) (2013) 731–738.
[37] W.S. Chow, et al., Effect of maleic anhydride-grafted ethylene–propylene rubber on the mechanical, rheological and morphological properties of organoclay reinforced polyamide 6/polypropylene nanocomposites, Eur. Polym. J. 41 (4) (2005) 687–696.
[38] B.-C. José, et al., Chemical modification of butyl rubber with maleic anhydride via nitroxide chemistry and its application in polymer blends, Polymers (Basel) 9 (2) (2017) 30970751.
[39] M.J. Azizli, et al., Hybrid rubber nanocomposites based on XNBR/EPDM: select the best dispersion type from different nanofillers in the presence of a compatibilizer, J. Inorg. Organomet. Polym. Mater. 30 (7) (2020) 2533–2550.
[40] L.-m. Wu, et al., Enhancement of mechanical properties of natural rubber with maleic anhydride grafted liquid polybutadiene functionalized graphene oxide, Chin. J. Polym. Sci. 33 (2015) 1058–1068.
[41] M. Hemmati, et al., Study on morphology, rheology and mechanical properties of thermoplastic elastomer polyolefin (TPO)/Carbon nanotube nanocomposites with reference to the effect of polypropylene-grafted-maleic anhydride (PP-g-MA) as a compatibilizer, Int. J. Polym. Mater. 60 (6) (2011) 384–397.
[42] S.-S. Choi, Difference in bound rubber formation of silica and carbon black with styrene-butadiene rubber, Polym. Adv. Technol. 13 (6) (2002) 466–474.

[43] S. Qian, et al., Investigation of carbon black network in natural rubber with different bound rubber contents, J. Macromol. Sci., Part B: Phys. 46 B (3) (2007) 453–466.
[44] G.M. Bristow, W.F. Watson, Cohesive energy densities of polymers. Part 1.-Cohesive energy densities of rubbers by swelling measurements, Trans. Faraday Soc. 54 (1958) 1731–1741, 0.
[45] A.J. Marzocca, Evaluation of the polymer–solvent interaction parameter χ for the system cured styrene butadiene rubber and toluene, Eur. Polym. J. 43 (6) (2007) 2682–2689.
[46] Characteristics and mechanical properties of composites based on nitrile butadiene rubber using graphene nanoplatelets 54(23), Compos Mater, 2020, p. 3351.
[47] M.A. Rafiee, et al., Fracture and fatigue in graphene nanocomposites, Small 6 (2) (2010) 179–183.
[48] M. Hernández, et al., Overall performance of natural rubber/graphene nanocomposites, Compos. Sci. Technol. 73 (2012) 40–46.
[49] S. Stankovich, et al., Graphene-based composite materials, Nature 442 (7100) (2006) 282–286.
[50] J. Wu, et al., Vulcanization kinetics of graphene/natural rubber nanocomposites, Polymer 54 (13) (2013) 3314–3323.
[51] M.J. Azizli, et al., Theoretical and experimental analyses of rheological, compatibility and mechanical properties of PVMQ/XNBR-g GMA/XNBR/GO ternary hybrid nanocomposites, Iran. Polym. J. (Engl. Ed.) 30 (10) (2021) 1001–1018.
[52] P. Ghosh, et al., Sulfur vulcanization of natural rubber for benzothiazole accelerated formulations: from reaction mechanisms to a rational kinetic model, Rubber Chem. Technol. 76 (3) (2003) 592–693.
[53] A. Tidjani, et al., Polypropylene–graft–maleic anhydride-nanocomposites: I—characterization and thermal stability of nanocomposites produced under nitrogen and in air, Polym. Degrad. Stabil. 82 (1) (2003) 133–140.
[54] M. Akiba, A.S. Hashim, Vulcanization and crosslinking in elastomers, Prog. Polym. Sci. 22 (3) (1997) 475–521.
[55] B. Mensah, et al., Preparation and characterization of rubber blends for industrial tire tread fabrication, International Journal of Polymer Science 2018 (2018), 2473286.
[56] S.-S. Choi, Effect of bound rubber on characteristics of highly filled styrene–butadiene rubber compounds with different types of carbon black, J. Appl. Polym. Sci. 93 (3) (2004) 1001–1006.
[57] J. Fröhlich, W. Niedermeier, H.D. Luginsland, The effect of filler–filler and filler–elastomer interaction on rubber reinforcement, Compos. Appl. Sci. Manuf. 36 (4) (2005) 449–460.
[58] B. Mensah, et al., A comparative study on vulcanization behavior of acrylonitrile-butadiene rubber reinforced with graphene oxide and reduced graphene oxide as fillers, Polym. Test. 76 (2019) 127–137.
[59] Z.-Y. Li, Y.-H. Song, Q. Zheng, Payne effect and weak overshoot in rubber nanocomposites, Chin. J. Polym. Sci. 40 (1) (2022) 85–92.
[60] X. Xiong, et al., Structure, thermal conductivity, and thermal stability of bromobutyl rubber nanocomposites with ionic liquid modified graphene oxide, Polym. Degrad. Stabil. 98 (11) (2013) 2208–2214.
[61] W. Xing, et al., Multifunctional properties of graphene/rubber nanocomposites fabricated by a modified latex compounding method, Compos. Sci. Technol. 99 (2014).
[62] R. Manna, S.K. Srivastava, Fabrication of functionalized graphene filled carboxylated nitrile rubber nanocomposites as flexible dielectric materials, Mater. Chem. Front. 1 (4) (2017) 780–788.
[63] Z. Dong, et al., Thermal property studies of in situ blended graphene/nature rubber nanocomposites, International Journal of Polymer Science 2020 (2020), 4694213.
[64] W. Xing, et al., Multifunctional properties of graphene/rubber nanocomposites fabricated by a modified latex compounding method, Compos. Sci. Technol. 99 (2014) 67–74.